Journal of Geophysical Research: Space Physics

RESEARCH ARTICLE
10.1029/2018JA025846

Statistical Study of Phase Relationship Between Magnetic and Plasma Pressures in the Near-Earth Nightside Magnetosphere Using the THEMIS-E Satellite

Katsuki Nishi[1], Kazuo Shiokawa[1], Karl-Heinz Glassmeier[2], and Johannes Z. D. Mieth[2]

[1]Institute for Space-Earth Environmental Research, Nagoya University, Nagoya, Japan, [2]Institut für Geophysik und extraterrestrische Physik, Technische Universität Braunschweig, Braunschweig, Germany

Key Points:
- Phase relation between variations of magnetic and plasma pressures in the nightside magnetosphere was statistically investigated
- The occurrence rates with coherence >0.85 are antiphase (39.75%) and in-phase (0.73%)
- Antiphase relationship is observed mainly at radial distances outside 8 R_E

Correspondence to:
K. Shiokawa,
shiokawa@nagoya-u.jp

Citation:
Nishi, K., Shiokawa, K., Glassmeier, K.-H., & Mieth, J. Z. D. (2018). Statistical study of phase relationship between magnetic and plasma pressures in the near-Earth nightside magnetosphere using the THEMIS-E satellite. *Journal of Geophysical Research: Space Physics*, *123*, 9517–9531. https://doi.org/10.1029/2018JA025846

Received 6 JUL 2018
Accepted 7 NOV 2018
Accepted article online 11 NOV 2018
Published online 28 NOV 2018

Abstract Distributions of plasma and magnetic pressures are the basic information to investigate macroscopic dynamics of the Earth's magnetosphere. Several studies have been made on magnetic and plasma pressures and macroscopic plasma instabilities in the magnetosphere. However, correlation between magnetic and plasma pressure variations has not been statistically investigated. In this paper, we analyze the statistical characteristics of the phase relationships between variations of magnetic and plasma pressures at frequencies of 4–15 mHz using 2 years of the THEMIS-E satellite data in the nightside magnetosphere. Spectral peaks with coherence greater than 0.85 between magnetic and plasma pressures for 1-hr time segments were selected. The average occurrence rates of the phase relationships are antiphase (within ±10° from 180°), 39.75%; in-phase (within ±10° from 0°), 0.73%; and other phases (10–170°), 49.83%. For the other-phase events, the phase differences are much closer to antiphase rather than to in-phase. Thus, we conclude that the two pressure variations tend to be antiphase. The antiphase and in-phase relationships are observed mainly at radial distances outside 8 R_E and inside 8 R_E, respectively. The high occurrence region of antiphase relationship is in the dawnside during magnetically quiet times and shifts to dusk side at active times defined as Dst < −10 nT. The occurrence rates of the phase relationships do not change significantly depending on the AE and Dst indices, plasma β, and IMF-B_z. Based on these results, we discuss the correspondence between the phase relationships and the possible magnetohydrodynamic force balances that can produce these phase relationships.

Plain Language Summary Distributions of plasma and magnetic pressures are the basic information to investigate macroscopic dynamics of the Earth's magnetosphere. Several studies have been made on magnetic and plasma pressures and macroscopic plasma instabilities in the magnetosphere. However, correlation between magnetic and plasma pressure variations has not been statistically investigated. In this paper, we analyze the statistical characteristics of the phase relationships between variations of magnetic and plasma pressures at frequencies of 4–15 mHz using 2 years of the THEMIS-E satellite data in the nightside magnetosphere. Spectral peaks with coherence greater than 0.85 between magnetic and plasma pressures for 1-hr time segments were selected. The average occurrence rates of the phase relationships are antiphase (39.75%), in-phase (0.73%), and other phases (49.83%). For the other-phase events, the phase differences are much closer to antiphase rather than to in-phase. Thus, we conclude that the two pressure variations tend to be antiphase in the nightside magnetosphere. We also investigate relation of these phase relationships with geomagnetic activities, solar wind parameters, and local times. Based on these results, we discuss the correspondence between the phase relationships and the possible magnetohydrodynamic force balances that can produce these phase relationships.

1. Introduction

Macroscopic plasma dynamics in the Earth's magnetosphere is basically described by the magnetohydrodynamics (MHD). In the idealized MHD equation of motion, the plasma acceleration occurs due to gradient forces of magnetic and plasma pressures and magnetic tension forces (e.g., Haerendel, 1990). Thus, it is important to investigate spatial distribution of magnetic and plasma pressures.

The magnetic and plasma pressures in the magnetosphere have been studied with various satellites (e.g., Behannon, 1968; Mihalov et al., 1968; Spence et al., 1989). Kistler et al. (1992) reported magnetic and plasma

pressures in the plasma sheet as a function of radial distances using the AMPTE/CCE satellite, focusing on periods before and after the onset of substorm-associated ion injection. Lui and Hamilton (1992) showed the radial profile of the parallel and perpendicular plasma pressures in the near-Earth plasma sheet during geomagnetically quiet time using the same satellite.

The reliable measurement of plasma pressure in the inner magnetosphere (inside ~10 R_E) is difficult, because the energies of plasma sheet ions tend to exceed the upper limit of the electrostatic analyzer (ESA; ~30 keV), getting into the energy range of the solid-state detector. Thus, measurements by both instruments and their cross calibration are essential for the reliable estimation of plasma pressures in the inner magnetosphere. The electrostatic analyzer (McFadden et al., 2008) and SST (solid-state telescope; Larson, 2009) onboard The Time History of Events and Macroscale Interactions during Substorms (THEMIS; Angelopoulos, 2008) satellites, which were launched in 2007, makes it possible to estimate the plasma pressures in the inner magnetosphere.

Macroscopic plasma instabilities are also important for our understanding of the dynamic variations of the magnetospheric plasma. Kinetic interchange or ballooning instabilities can play an important role in the dynamic motion of the magnetospheric plasma (e.g., Gold, 1959). Both instabilities may develop in the region where the earthward tension force and tailward pressure-gradient forces balance. We can analyze these macro-scale plasma instabilities using conjugate ground-based and magnetospheric measurements of auroras (e.g., Motoba et al., 2015; Voronkov et al., 2000; Safargaleev et al., 2003). In addition, earthward plasma flow in the tail plasma sheet can also cause diamagnetic variations in the inner magnetosphere as compressional waves. Runov et al. (2014) and Liu et al. (2017) showed diamagnetic antiphase variations in magnetic and plasma pressures prior to the arrival of dipolarization front in the tail plasma sheet, indicating that plasma compression by earthward flow propagated farther inward and excited compressional diamagnetic oscillations.

Pressure-driven instability between plasma and magnetic pressures was suggested as a possible mechanism of auroral fragmentations into patches (Shiokawa et al., 2010; Shiokawa et al., 2014). Shiokawa et al. (2010, 2014) regarded auroral finger-like structures, which we can see in diffuse auroral regions during the auroral fragmentations as manifestations of the pressure-driven instability in the magnetosphere. Recently, Nishi et al. (2017, 2018) reported two simultaneous observations of the auroral finger-like structures using ground-based all-sky imagers and satellites in the magnetosphere. One used the THEMIS-E satellite at a radial distance of ~8 R_E and the other used the RBSP-A satellite at a radial distance of ~5.5 R_E. In the former event, they found clear antiphase fluctuations between the plasma and magnetic pressures during the conjunction period. This result is consistent with the idea of the pressure-driven instability advocated by Shiokawa et al. (2010, 2014). However in the latter event (Nishi et al., 2018), the phase relationship of the pressure fluctuations was not systematic, differently from the THEMIS-E conjunction event. This difference of phase relationship of plasma and magnetic pressures between THEMIS-E (~8 R_E) and RBSP-A (~5.5 R_E) associated with auroral finger-like structures provided us a strong motivation to systematically investigate the correlation of these pressure variations in the nightside magnetosphere. However, correlation between magnetic and plasma pressure variations have not been statistically studied in the near-Earth magnetosphere. In this paper, we investigate the statistical characteristics of the phase relationships between variations of magnetic and plasma pressures using 2 years of the THEMIS-E satellite data and their dependences on local time, geomagnetic activities, plasma β, and IMF-B_Z.

2. Statistical Data Set and Analysis Method

In this study, we used 2-year plasma and magnetic field data obtained from the THEMIS-E satellite from 1 February 2011 to 1 February 2013. The solar wind parameters used in this study were obtained from the ACE satellite. We calculated perpendicular plasma pressures using the ions data from ESA and SST with energy ranges of 5 eV to 25 keV and 25 keV to 1 MeV, respectively. We did not use electron pressure in this analysis, because the ion pressure is usually much higher than the electron pressure. We also calculated magnetic pressures using the fluxgate magnetometer (FGM; Auster et al., 2008) instrument onboard the THEMIS-E satellite. Time resolutions of both plasma and magnetic field data are ~3 s.

Using these magnetic field and plasma data, we made the following analysis procedures to obtain the phase relationship of the magnetic and plasma pressures. (1) We subtracted 10-min running averages of the pressures data from the original data in order to extract variation components with periods of several minutes which are comparable with the time scales of finger-like structure crossings reported by

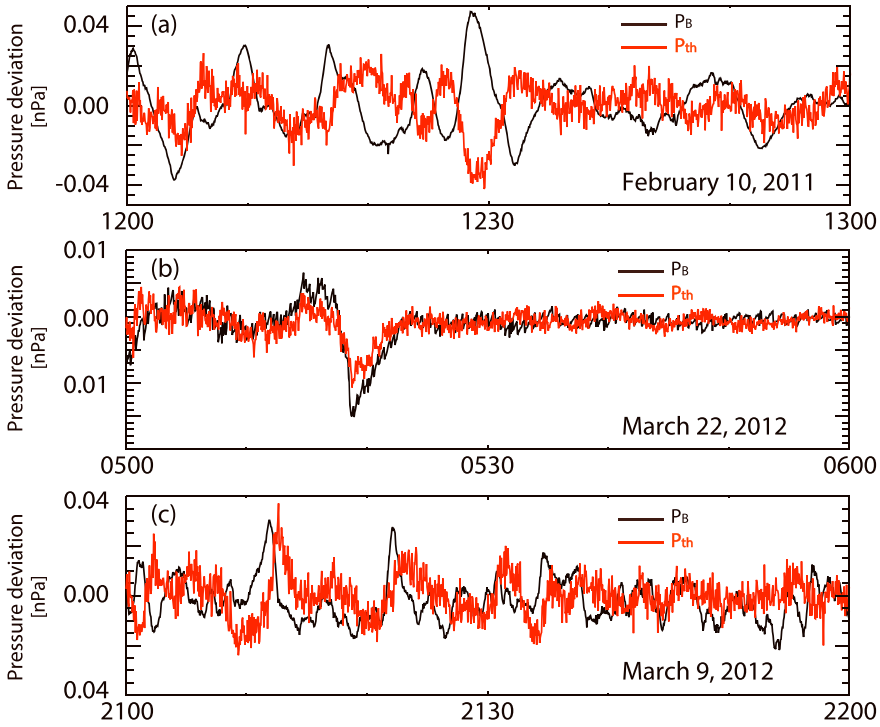

Figure 1. Examples of the phase relationships between ΔP_{th} and ΔP_B. (a–c) The examples of antiphase, in-phase, and other phases, respectively.

Nishi et al. (2017, 2018). (2) For every 1-hr time segments with 1,201 or 1,202 data points, we calculated power spectra of the variation components of the plasma and magnetic pressures, ΔP_{th} and ΔP_B, respectively, and coherences and phases between these pressures using the fast Fourier transform (FFT). In this FFT procedure, we used a cosine window for 1/10th of both side edges of the 1,201 or 1,202 data to reduce the edge effect before the FFT, and multiply 1/0.875 for the output spectra to compensate this cosine window effect. The original number of data is enhanced to 32,768 by adding zero data before and after the 1-hr data, in order to apparently increase the spectral resolution. After the FFT, we took a running average of eight data points of the power spectra in the frequency domain, making the degree of freedom of 16. (3) We searched local peaks in the power spectra of ΔP_{th} and ΔP_B at same frequencies, and selected the peaks whose coherence between ΔP_{th} and ΔP_B are greater than 0.85. (4) For the selected power spectra peaks with high coherence, we classified phase relationships between ΔP_{th} and ΔP_B into the following 3 types: antiphase, in-phase and other-phase, which are defined as:

$$\text{antiphase}: -180^\circ < \theta < -170^\circ, 170^\circ < \theta < 180^\circ \quad (1)$$

$$\text{in-phase}: -10^\circ < \theta < 10^\circ \quad (2)$$

$$\text{other-phase}: -170^\circ < \theta < -10^\circ, 10^\circ < \theta < 170^\circ \quad (3)$$

where θ is the phase obtained from the FFT. Note that the peaks at frequencies below 4 mHz are ignored in the analysis in order to remove artificial peaks caused by the subtraction of 10-min averages. We also ignored the data segments whose 1-h average ion velocities in Geocentric Solar Magnetospheric (GSM) $\mp x$ direction exceeded −200 km/s, regarding them as observation of the solar wind not that of the magnetosphere. Because we calculate coherence for each 1-hr data segment, events with durations much shorter than 1 hr, such as dipolarization front, would be difficult to satisfy our selection criteria.

Figure 1 shows examples of the phase relationships between ΔP_{th} and ΔP_B. From top to bottom, the examples of antiphase, in-phase, and other phases are shown. In Figure 1a, we can see clear antiphase fluctuations between the black and red curves in various time scales. In Figure 1b, ΔP_{th} and ΔP_B show similar variations in particular before 0530 UT. In Figure 1c, ΔP_{th} varies independently from ΔP_B.

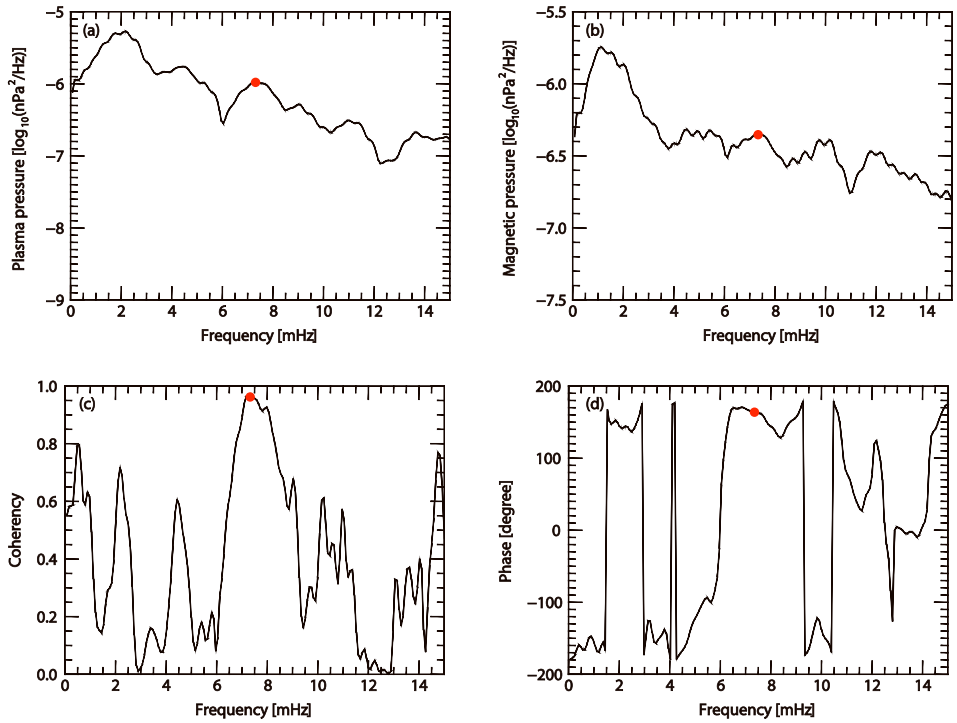

Figure 2. Examples of the power spectra of (a) ΔP_{th} and (b) ΔP_B, (c) coherence, and (d) phase obtained from the FFT analysis for the data of 10 February 2011 at 1200–1300 UT.

Figure 2 shows examples of the power spectra of (a) ΔP_{th} and (b) ΔP_B, (c) coherence and (d) phase obtained from the FFT analysis for the data of 10 February, 2011 at 1200–1300 UT shown in Figure 1a. Red dots in Figure 2 indicate the peak of power spectra detected by our procedure. In panels (a) and (b), we can see the spectral peaks at the same frequency of ~7.5 mHz. According to panels (c) and (d), the coherence is greater than 0.85 and the phase is ~ 180° at ~7.5 mHz. Therefore, we classified that this data segment contains an antiphase oscillation.

3. Results

Figure 3 shows the histograms of the phase relationships. Red, blue and green lines indicate the number of spectral peaks with coherence >0.85 for antiphase, in-phase, and other phases, respectively as a function of frequency. We ignored shaded area in Figure 3 as mentioned in section 2 to avoid artificial spectral peaks due to subtraction of 10-min running averages. Numbers in parenthesis indicate the total numbers of spectral peaks with coherence >0.85 plotted in this figure for frequencies between 4 and 15 mHz. The numbers of in-phase events are very small compared with out-of-phase and other-phase events. In Figure 3a, the number of events decreases with increasing frequencies from 4 to 15 mHz without outstanding peaks. Figures 3b and 3c indicate a Dst-index dependence of these phase relationships divided by Dst smaller and larger than −10 nT. The number of antiphase events at lower frequencies increase during geomagnetically quiet time at Dst > −10 nT.

Figure 4 shows the histogram of the number of spectral peaks for different phases. The horizontal axis indicates the phase difference between ΔP_{th} and ΔP_B. The vertical axis indicates the number of spectral peaks with coherence >0.85. The bin size of the horizontal axis is 10° . We cannot see many events for phase relationships within ±100°. On the other hand, the number of spectral peaks increase drastically as approaching to the antiphase relationship of ±180°. This figure indicates that the events categorized as *other phase* are mostly close to the antiphase relationship.

Figure 5 shows the distribution of occurrence rates of phase relationships for (a) antiphase, (b) in-phase, and (c) other phases, and (d) the distribution of number of THEMIS-E passes in the GSM *x*-*y* plane of the magnetosphere. A scale size of a grid in Figure 5 is 1 R_E square. According to Figure 5d, the number of the passes is

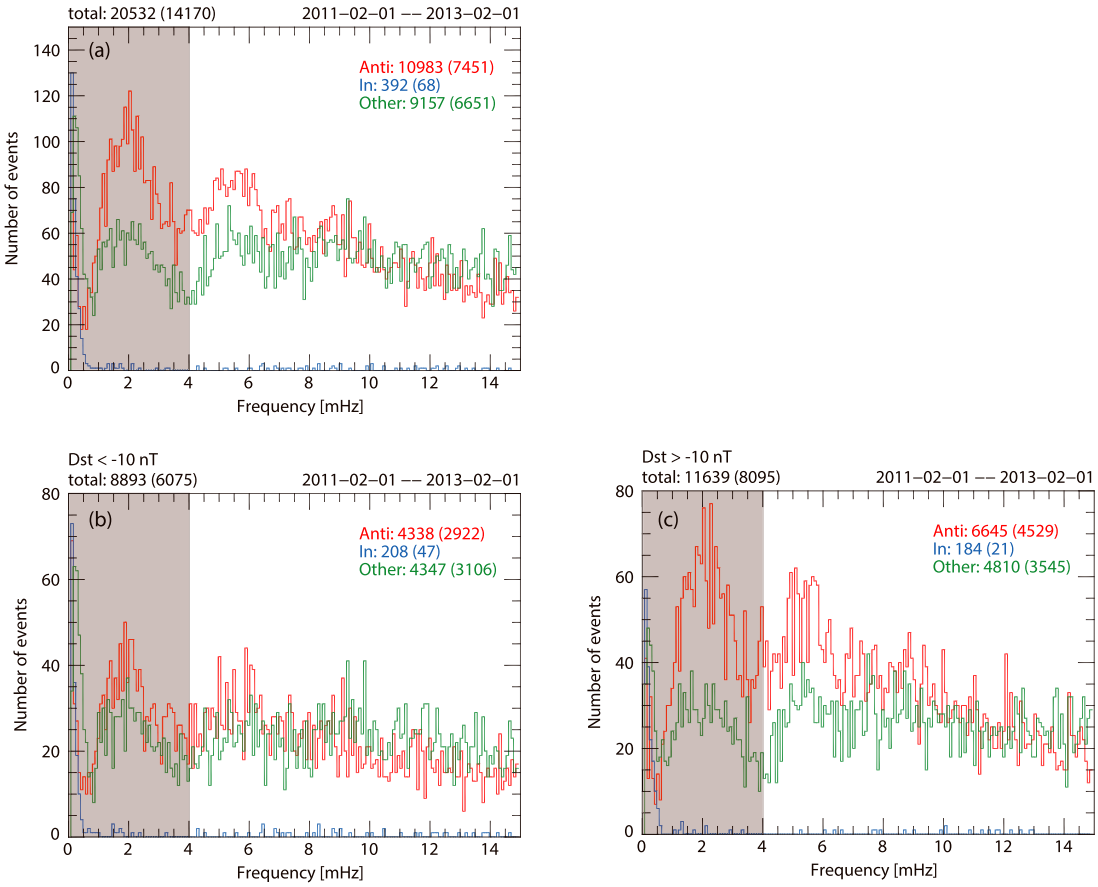

Figure 3. Histograms of the number of phase relationships. Red, blue and green lines indicate antiphase, in-phase, and other phases, respectively. Numbers in parenthesis indicate the total numbers of spectral peaks with coherence >0.85 plotted in this figure for frequencies between 4 and 15 mHz.

greater than 20 in most of the grid in orbits of the THEMIS-E satellite. These occurrence rates were calculated by dividing the number of high-correlation events by the number of passes for each grid. Total numbers of the phase relationships are, for antiphase, 2728; for in-phase, 51; and for other phases, 3426. If one 1-hour data segment is classified into more than two phase relationships at different frequencies, we count the number of each phase relationship separately. If one 1-hr segment has more than two antiphase/in-phase/other-phase peaks, we counted it as one antiphase/in-phase/other-phase event. Thus, one 1-hr segment can be counted maximum three times, if there are three frequency peaks with antiphase, in-phase, and other phases.

In Figure 5a, the occurrence rates of antiphase events increase at midnight and the dusk and dawn flanks near the apogee of the THEMIS-E satellite. The occurrence rates exceed 40% in most of the grid between 8 and 12 R_E. On the other hand, the occurrence rates significantly decrease in the near-earth region between 4 and 6 R_E. The occurrence rate of in-phase events is quite small and mostly occurs within 8 R_E in contrast to the antiphase events. The occurrence rate distribution of other-phase is similar to that of antiphase events. However, the other-phase occurrence rate is larger than the antiphase occurrence rate inside 8 R_E.

Figure 6 shows the cross sections of Figures 5a–5c at dusk (1800–2200 LT), midnight (2200–0200 LT), and dawn (0200–0600 LT). The color configurations are same as Figure 3, that is, red, blue, and green lines indicate the occurrence rates for antiphase, in-phase, and other phases, respectively. According to Figure 6, as the radial distance increases, the occurrence rates of the antiphase and other phases tend to increase up to more than 50% at radial distances of more than 10 R_E. The occurrence rate of the other-phase is greater than that of the antiphase at almost all the radial distances.

Figures 7 and 8 show the Dst dependence of the occurrence rate distributions of the phase relationships divided by Dst = −10 nT. The figure format is same as that of Figure 5. The number of passes of Dst < −10 nT and Dst > −10 nT are fairly comparable each other. During geomagnetically active time with Dst < −10 nT

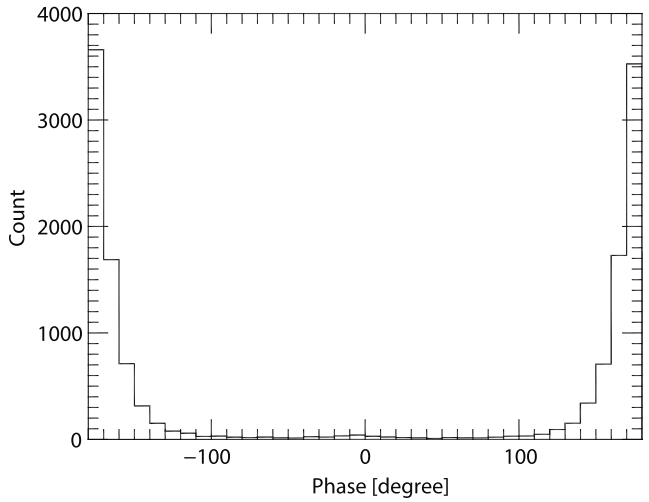

Figure 4. Histogram of the number of spectral peaks with coherence >0.85 as binned according to the phase difference between ΔP_{th} and ΔP_B.

(Figure 7), we can see high occurrence region of the antiphase in the dusk sector. The high occurrence region shifts to the dawn side during the quite time with Dst > −10 nT (Figure 8). There is little difference of the in- and other-phases between Dst < −10 nT and Dst > −10 nT. Similar dependence of occurrence rate distribution was obtained when we sort the events by the AE index and IMF-B_z.

Figures 9 and 10 show the dependence of the occurrence rates of the phase relationships on plasma β divided by $\beta = 1$. The average β of each 1-hour time segment is used as representative value of the segment. Generally speaking, the region of $\beta > 1$ can be considered as the plasma sheet, while the region of $\beta < 1$ can be either the plasma sheet boundary layer or the lobe. The number of passes in low-β condition is more than twice as many as that in high-β condition. In Figure 9d, we can see many high-β passes in the dawn and dusk flanks of the magnetosphere. This feature is consistent with a result of the statistical study of β distribution using the ISEE spacecraft data reported by Zhu and Kivelson (1991). On the other hand, for the low-β regions, the number of passes increases at midnight. The occurrence rate of the antiphase events in the dawn and dusk flanks are higher than that of the antiphase events around midnight at radial distance of ~10 R_E in the high-β condition in Figure 9a. In the low-β condition in Figure 10a, this local time distribution of the antiphase occurrence rate becomes opposite to that in the high-β condition. In Figures 9b and 10b, most of the in-phase events are observed in the low-β condition. Anyhow, the occurrence rate of the in-phase events is less than 10% even under the low-β condition.

Figure 11 indicates the number of 1-hr time segments (passes) that satisfy the criteria of drift mirror instability for more than half (30 min) of the 1-hr time segment. The criteria of drift mirror instability are $\sum_s \frac{\beta_{s\perp}^2}{\beta_{s\parallel}} > 1 + \sum_s \beta_{s\perp}$ (e.g., Treumann & Baumjohann, 1997), where $\beta_{s\parallel}$ and $\beta_{s\perp}$ are parallel and perpendicular β values for particles of s-type (ions and electrons). In Figure 11, only ~5% of the total of passes satisfy the drift mirror criteria. Therefore, most of the antiphase events shown in Figure 5a are observed under the condition when the drift-mirror mode cannot develop in the magnetosphere.

Table 1 summarizes the occurrence rates of the antiphase, in-phase, and other-phase relationships between ΔP_{th} and ΔP_B, and their dependence on the AE and Dst indices, plasma β and IMF-B_z. These occurrence rates are derived by the divisions of the total number of passes and the number of events in each condition. According to the second column, the occurrence rates of the antiphase events are 36–43%, indicating that the antiphase fluctuations between the plasma and magnetic pressures are frequently observed in the nightside magnetosphere. On the other hand, the occurrence rates of the in-phase events are quite small. The occurrence rates do not vary significantly depending on these parameters of AE and Dst indices, plasma β, and IMF-B_z.

Table 1
Occurrence Rates of the Antiphase, In-Phase, and Other-Phase Relationships and Their Dependence of the AE and Dst Indices, Plasma β, and IMF-B_z

	Antiphase (%)	In-phase (%)	Other phases (%)
Total	39.75	0.73	49.83
AE > 100 nT	41.44	0.88	54.44
AE < 100 nT	37.40	0.55	44.11
Dst < −10 nT	36.91	0.88	49.82
Dst > −10 nT	42.35	0.59	49.85
$\beta > 1$	43.57	0.31	54.38
$\beta < 1$	40.41	0.95	50.78
IMF-$B_z < 0$	39.88	0.64	53.37
IMF-$B_z > 0$	37.35	0.66	46.83

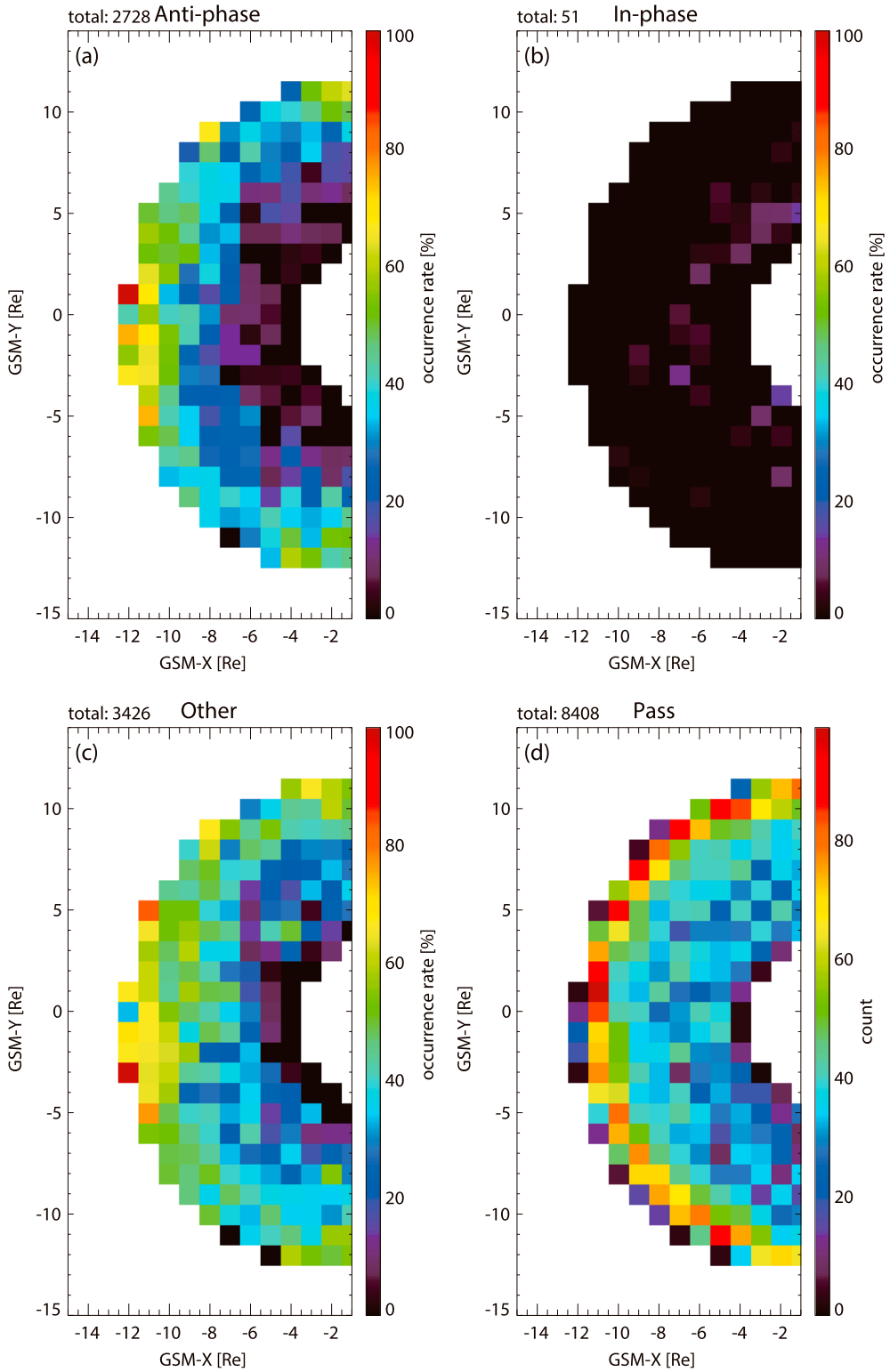

Figure 5. Occurrence rates of phase relationships and the number of passes of THEMIS-E distributions in the GSM *x*-*y* plane of the magnetosphere. (a), (b), and (c) are occurrence rates distribution of antiphase, in-phase, and other phases, respectively. (d) indicates the number of passes of the THEMIS-E satellite.

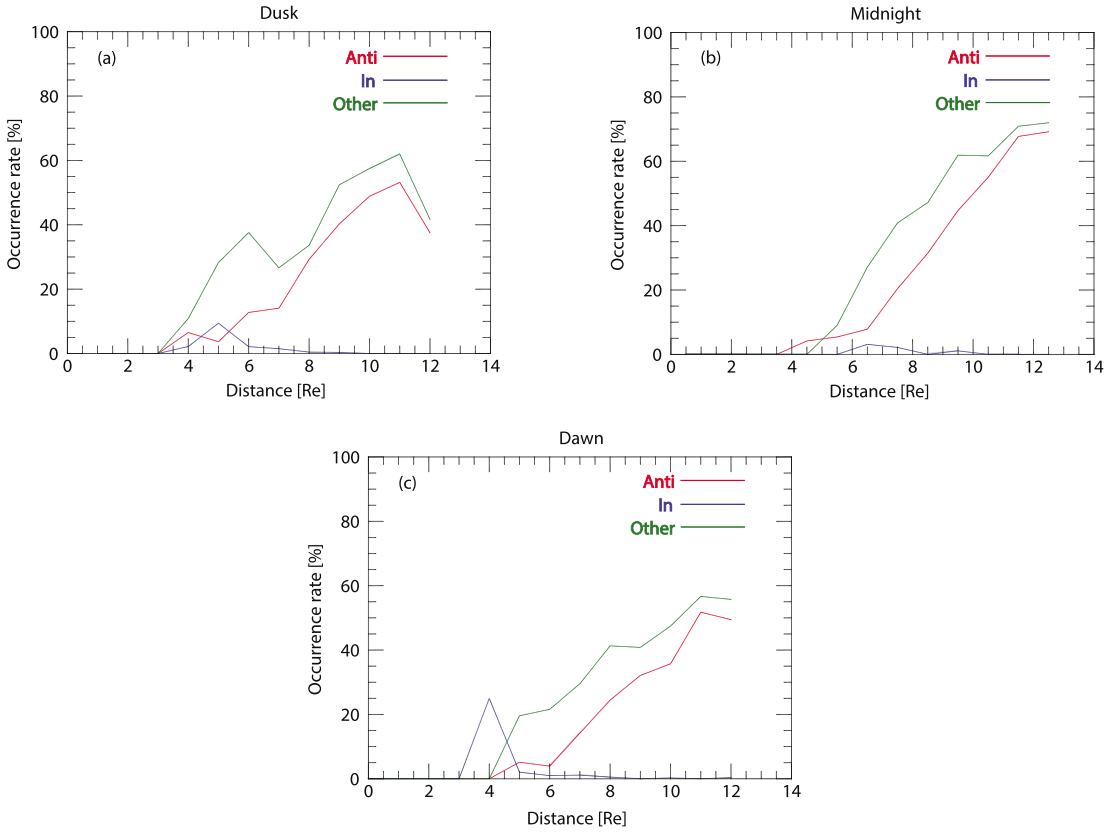

Figure 6. Cross sections of the Figure 5 at (a) dusk (1800–2200 LT), (b) midnight (2200–0200 LT), and (c) dawn (0200–0600 LT). The color configurations are same as Figure 3. The horizontal axis indicates the radial distance from the earth.

4. Discussion

We have reported a statistical study of the phase relationships between fluctuations of the plasma and magnetic pressures at a frequency range of 4–15 mHz in the nightside magnetosphere using the THEMIS-E satellite over a period of 2 years from 1 February 2011 to 1 February 2013. From this analysis, we found several interesting characteristics about the occurrence rate distributions of the antiphase, in-phase, and other-phase events and their dependences on geomagnetic activities and plasma β.

Excitation mechanisms of electromagnetic pulsations in this ULF range may be roughly divided into four types: (1) the ULF variability in the solar wind parameters, (2) instabilities on the magnetopause, (3) ULF instabilities of the magnetospheric plasma population (e.g., Takahashi & Ukhorskiy, 2007), and (4) flapping of the plasma sheet (e.g., Sergeev et al., 2003; Runov et al., 2005). In Figure 8, we can see the high occurrence region of the antiphase events mainly in the midnight far from the magnetopause. Thus we considered that the source mechanism of the antiphase fluctuations is either the ULF instabilities of the magnetospheric plasma populations or plasma sheet flapping. The drift mirror instability can be a candidate of the source mechanism of the ULF range antiphase fluctuations. However, the drift mirror mode criteria are not satisfied during most of our observational period (<5%), although the antiphase fluctuations are frequently observed (>36–43%). We need more study to identify the source mechanisms of the antiphase ULF oscillations in order to explain the frequent antiphase fluctuations between the plasma and magnetic pressures at the present frequency range.

As shown in Figures 9 and 10 and Table 1, we can see the antiphase relationships frequently for both high- and low-β regions. However, in the inner magnetosphere within 4–8 R_E where strong magnetic fields exist, the occurrence rate of the antiphase events drastically decreases. This feature may be explained by the MHD momentum equation written as

$$nm\frac{d\vec{v}}{dt} = -\vec{\nabla}(P_{th} + P_B) + \frac{1}{\mu_0}(\vec{B}\cdot\vec{\nabla})\vec{B} \tag{4}$$

where n, m, $\vec{v}$, and μ_0 are the plasma number density, mass (mainly ion mass), bulk velocity, and permeability

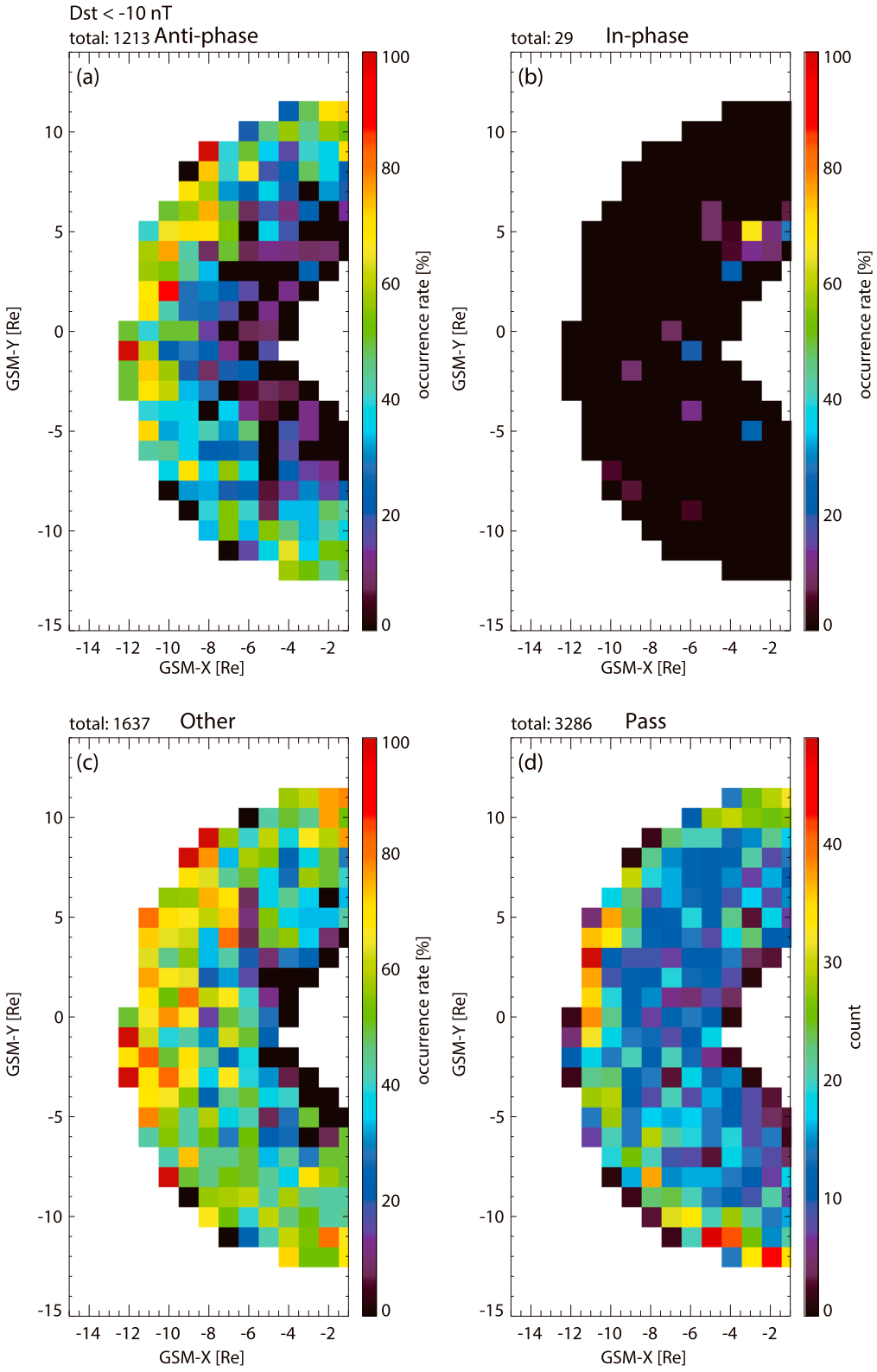

Figure 7. Occurrence rates of phase relationships and the number of passes of THEMIS-E distributions in the GSM *x*-*y* plane of the magnetosphere when Dst < −10 nT. The format of this figure is same as that of Figure 5.

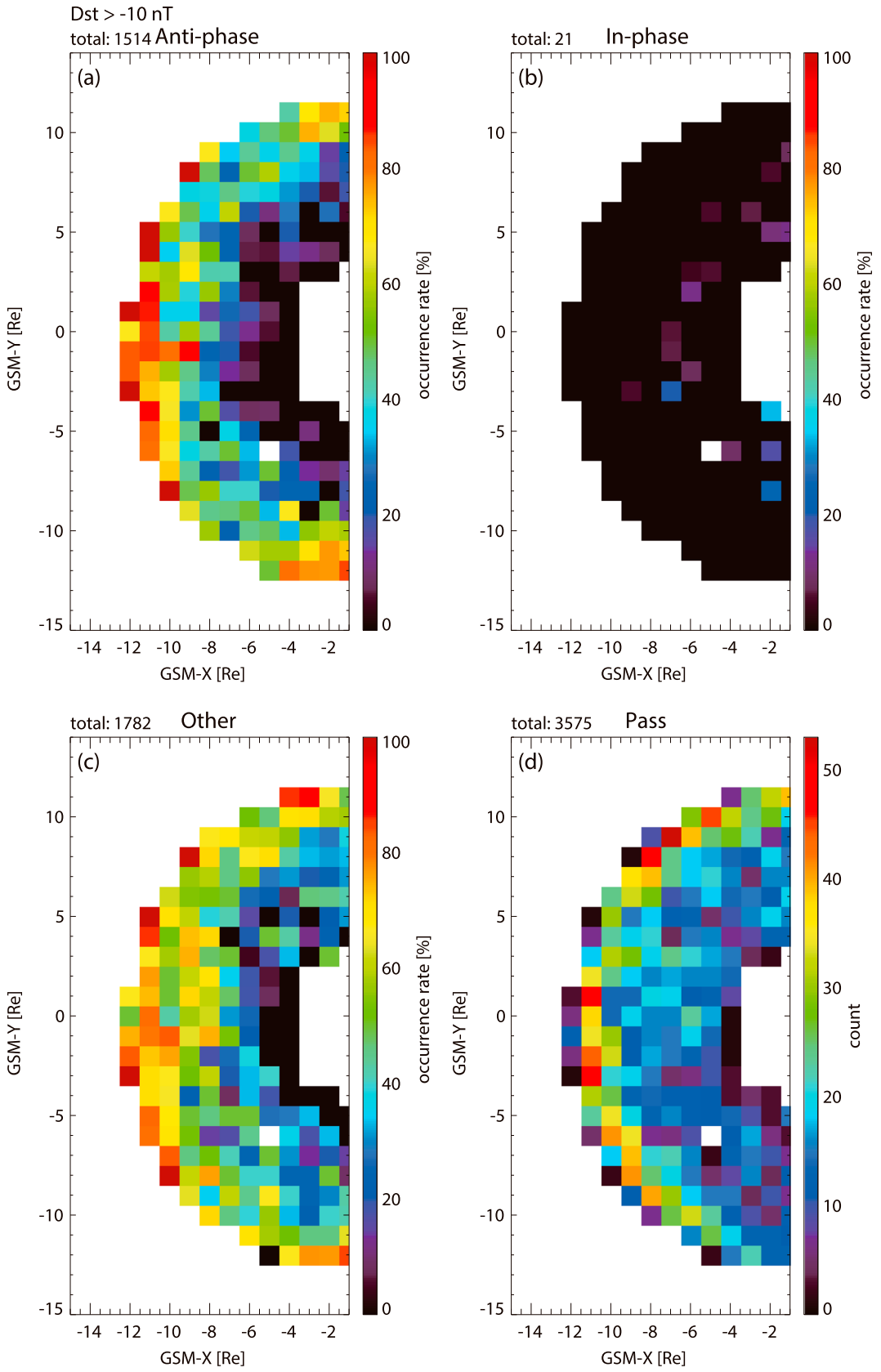

Figure 8. The same as Figure 7 but for Dst > −10 nT.

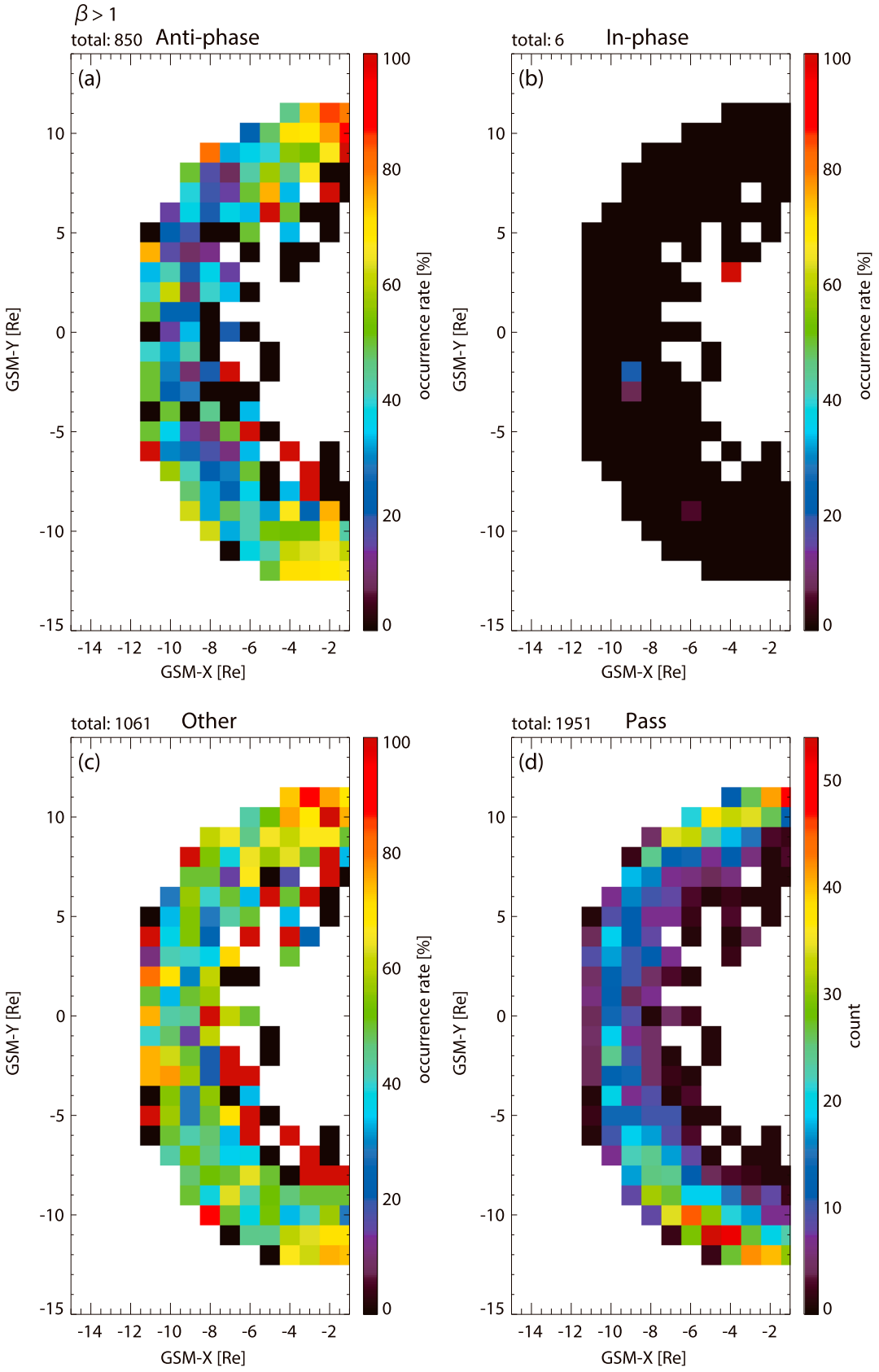

Figure 9. The same as Figure 7 but $\beta > 1$.

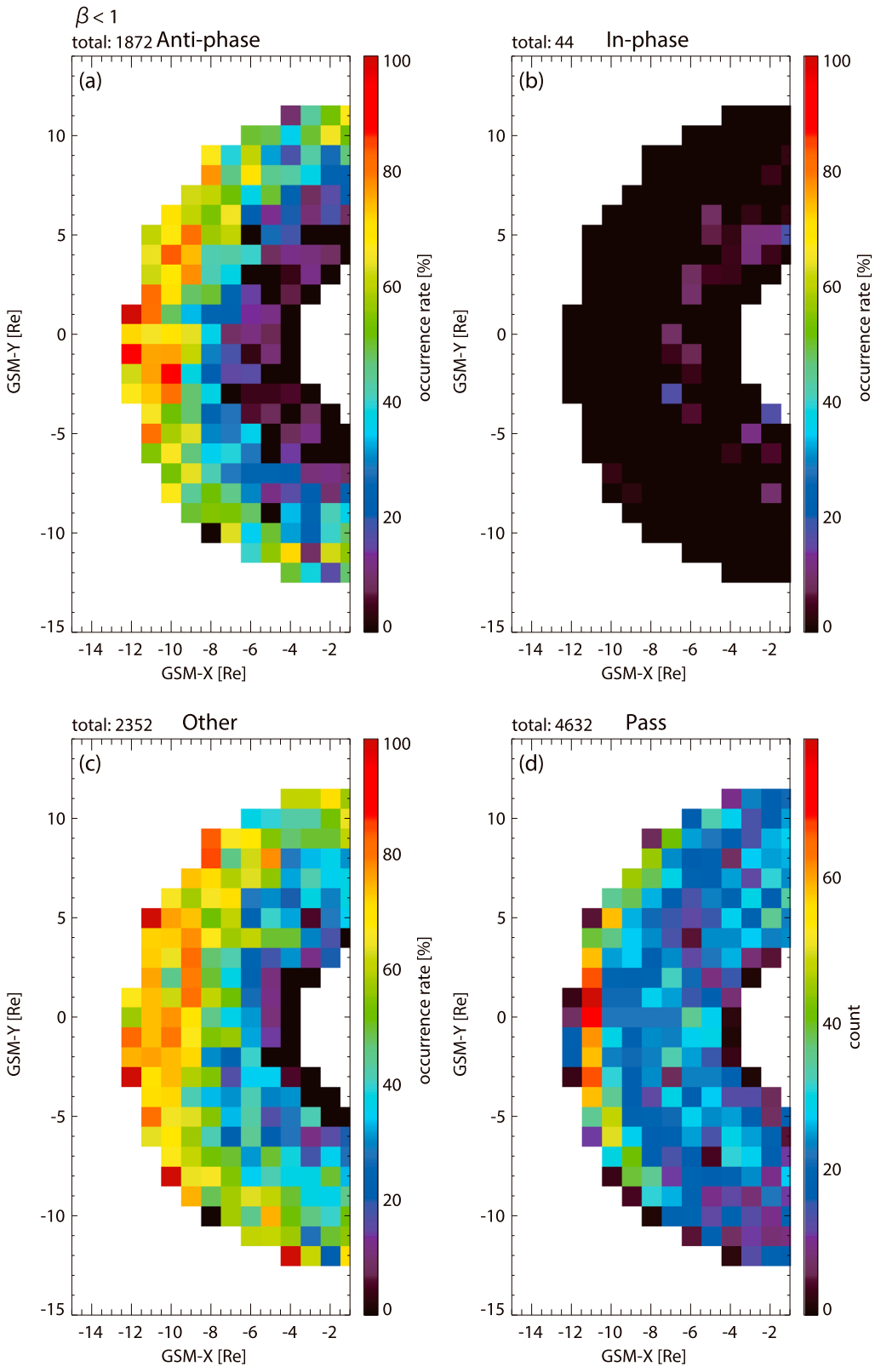

Figure 10. The same as Figure 7 but $\beta < 1$.

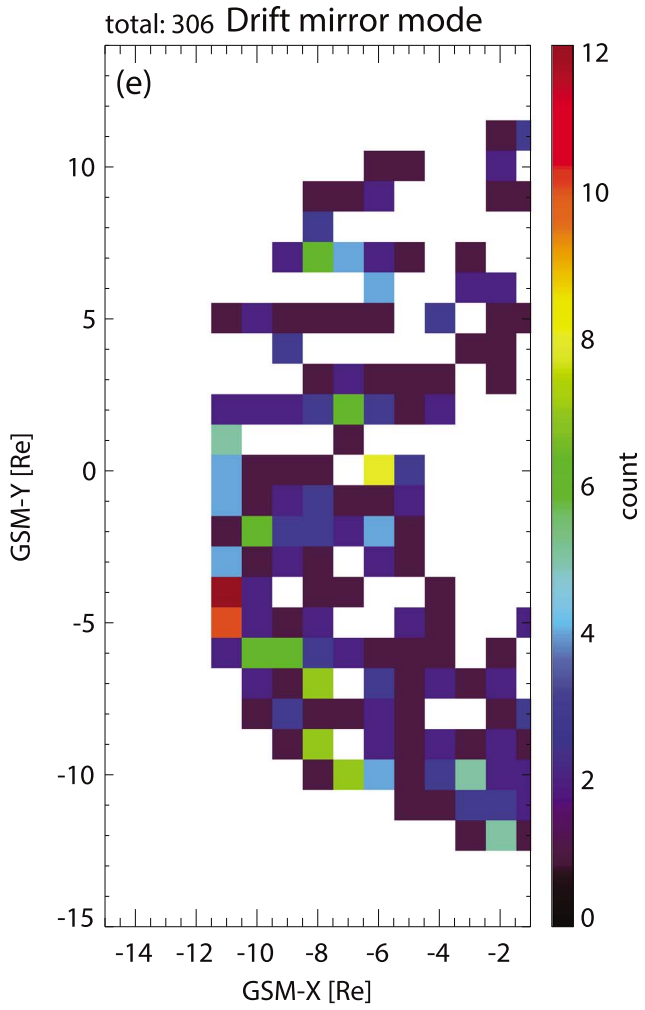

Figure 11. The number of the passes which satisfy the criteria of drift mirror instability for more than half (30 min) of the 1-hr time segment.

in vacuum, respectively (e.g., Haerendel, 1990). If the acceleration of the plasma is small enough to be neglected, the MHD force balance is kept between the pressure gradient and magnetic tension forces, according to equation (4). Additionally, if the magnetic tension force also small enough compared with the pressure gradient force, the plasma and magnetic pressure gradient forces fluctuate in antiphase. Thus, the antiphase oscillations would not be observed when the plasma β is very small or the curvature of the magnetic field is significant. This consideration is consistent with the observational fact that the antiphase relationship tends to be not observed in the inner magnetosphere. The occurrence rate of the antiphase events slightly increases in high-β condition, as shown in Table 1.

On the other hand, we observed the in-phase relationship mainly in the inner magnetosphere within 4–8 R_E contrary to the antiphase relationship. The magnetic fields and their curvature are probably large enough to produce strong magnetic tension forces compared with the pressure gradient forces in this region. In that case, it may be possible that the plasma and magnetic pressures increase simultaneously in order to balance with the magnetic tension force. However, the occurrence rate of the in-phase variation is less than 10% even if it is in the inner magnetosphere. The force balance against the magnetic tension force may be mainly by the magnetic pressure gradient force, and the contribution of the plasma pressure would be minor in the inner magnetosphere.

Now we discuss the Dst dependence of the occurrence rates of the phase relationships. As shown in Figures 7 and 8, the high occurrence region of the antiphase events is in the dawn side at magnetically quite time ($Dst > -10$ nT) and it shifts to the dusk side at $Dst < -10$ nT. The cause of the shift of high occurrence region is

probably related to the plasma injection associated with magnetic disturbances. Ions injected from the magnetotail rotate westward in the dipolar magnetic field configuration in the magnetosphere (e.g., Baumjohann & Treumann, 1996). The westward injected ions increase the plasma β in the duskside, which also increase the occurrence rate of the antiphase events there. This consideration does not contradict to the result of the plasma β dependence shown in Table 1.

5. Conclusion

In this paper, we statistically analyzed the phase relationships between the plasma and magnetic pressures at a frequency range of 4–15 mHz and their dependence on local time, geomagnetic activities, plasma β, and IMF-B_z. From this statistical analysis we obtained observational facts as follows:

1. The two pressure variations tend to be antiphase. The average occurrence rates of the phase relationships are, for antiphase, 39.75%; for in-phase, 0.73%; and for other-phase, 49.83%. For the other-phase events, the phase differences are closer to antiphase rather than to in-phase.
2. The antiphase and in-phase relationships are observed mainly at radial distances outside 8 R_E and inside 8 R_E, respectively.
3. The high occurrence region of phase is the dawnside at magnetically quiet times and shifts to dusk side at active times defined as Dst < -10 nT.
4. The occurrence rates of the phase relationships do not change significantly depending on the AE and Dst indices, plasma β and IMF-B_z.

Based on these results, we discussed the correspondence between the phase relationships and the possible MHD force balances which produce these phase relationships. However, there is still room for considering the source mechanisms of this antiphase fluctuations in ULF-frequency range, which can be either ULF instabilities or plasma sheet flapping. Moreover, we have not derived information related to the pressure-driven instability or the auroral finger-like structures from present statistical analysis. A further direction of this study will be to analyze more conjugate or near-conjugate observations of the auroral finger-like structures in order to obtain more information about conditions of the appearance of auroral finger-like structures. The result of this paper would strengthen the understanding of the generation mechanism of the auroral finger-like structures by providing background information of antiphase oscillations between magnetic and plasma pressures.

Acknowledgments
We acknowledge NASA contract NAS5-02099 and V. Angelopoulos for the use of data from the THEMIS mission. Specifically, we thank C. W. Carlson and J. P. Mcfadden for use of ESA data; D. Larson for use of SST data; K. H. Glassmeier, U. Auster, and W. Baumjohann for the use of FGM data provided under the lead of the Technical University of Braunschweig and with financial support through the German Ministry for Economy and Technology and the German Center for Aviation and Space (DLR) under contract 50 OC 0302. THEMIS probes data are available through the open data repository at UC Berkeley at http://themis.ssl.berkeley.edu/index.shtml. We also acknowledge use of NASA/GSFC Space physics Data Facility OMNIWeb (http://omniweb.gsfc.nasa.gov) service, and OMNI data. This work was supported by KAKENHI grants JP 15H05815 and JP 16H06286 provided by the Japan Society for the Promotion of Science.

References

Angelopoulos, V. (2008). The THEMIS mission. *Space Science Reviews*, *141*, 5–34. https://doi.org/10.1007/s11214-008-9336-1

Auster, H. U., Glassmeier, K. H., Magnes, W., Aydogar, O., Baumjohann, W., Constantinescu, D., et al. (2008). The THEMIS fluxgate magnetometer. *Space Science Reviews*, *141*, 235–264. https://doi.org/10.1007/s11214-008-9365-9

Baumjohann, W., & Treumann, R. A. (1996). *Basic Space Plasma Physics*. London: Imperial College Press.

Behannon, K. (1968). Mapping the Earth's bow shock and magnetic tail by Explorer 33. *Journal of Geophysical Research*, *73*, 907.

Gold, T. (1959). Motions in the magnetosphere of the Earth. *Journal of Geophysical Research*, *64*(9), 1219–1224.

Haerendel, G. (1990). Field-aligned currents in the Earth's magnetosphere. In C. T. Russell, E. R. Priest, & L. C. Lee (Eds.), *Physics of magnetic flux ropes, Geophysical of Monograph Series* (Vol. *58*, pp. 539–553). Washington, DC: American Geophysical Union.

Kistler, L. M., Möbius, E., Baumjohann, W., Paschmann, G., & Hamilton, D. C. (1992). Pressure changes in the plasma sheet during substorm injections. *Journal of Geophysical Research*, *97*, 2973.

Larson, D. (2009). Using the THEMIS energetic particle data. Retrieved from http://www.virbo.org/Image:THEMIS-SST.pp

Liu, J., Angelopoulos, V., Zhang, X.-J., Runov, A., Artemyev, A., Plaschke, F., et al. (2017). Ultralow frequency waves deep inside the inner magnetosphere driven by dipolarizing flux bundles. *Journal of Geophysical Research: Space Physics*, *122*, 10–112. https://doi.org/10.1002/2017JA024270

Lui, A. T. Y., & Hamilton, D. C. (1992). Radial profiles of quiet time magnetospheric parameters. *Journal of Geophysical Research*, *97*(A12), 19,325–19,332.

McFadden, J. P., Carlson, C. W., Larson, D., Ludlam, M., Ablad, R., Elliott, B., et al. (2008). The THEMIS ESA plasma instrument and in-flight calibration. *Space Science Reviews*, *141*, 277–302. https://doi.org/10.1007/s11214-008-9440-2

Mihalov, J. D., Colburn, D. S., Currie, R. G., & Sonett, C. P. (1968). Configuration and reconnection of the geomagnetic tail. *Journal of Geophysical Research*, *73*, 943.

Motoba, T., Ohtani, S., Donovan, E. F., & Angelopoulos, V. (2015). On a possible connection between the longitudinally propagating near-Earth plasma sheet and auroral arc waves: A reexamination. *Journal of Geophysical Research: Space Physics*, *120*, 432–444. https://doi.org/10.1002/2014JA020694

Nishi, K., Shiokawa, K., & Frühauff, D. (2017). Conjugate observation of auroral finger-like structures by ground-based all-sky cameras and THEMIS satellites. *Journal of Geophysical Research: Space Physics*, *122*, 7291–7306. https://doi.org/10.1002/2016JA023774

Nishi, K., Shiokawa, K., & Spence, H. E. (2018). Magnetospheric source region of auroral finger-like structures observed by the RBSP-a satellite. *Journal of Geophysical Research: Space Physics*, *123*, 7513–7522. https://doi.org/10.0002/2018JA025480

Runov, A., Runov, A., Sergeev, V. A., Baumjohann, W., Nakamura, R., Apatenkov, S., et al. (2005). Electric current and magnetic field geometry in flapping magnetotail current sheets. *Annals of Geophysics*, *23*, 1391–1403.

Runov, A., Sergeev, V. A., Angelopoulos, V., Glassmeier, K.-H., & Singer, H. J. (2014). Diamagnetic oscillations ahead of stopped dipolarization fronts. *Journal of Geophysical Research: Space Physics*, *119*, 1643–1657. https://doi.org/10.1002/2013JA019384

Safargaleev, V. V., Kozlovsky, A. E., Osipenko, S. V., & Tagirov, V. R. (2003). Azimuthal expansion of high-latitude auroral arcs. *Annales de Geophysique*, *21*, 1793–1805.

Sergeev, V., Sergeev, V., Runov, A., Baumjohann, W., Nakamura, R., Zhang, T. L., et al. (2003). Current sheet flapping motion and structure observed by Cluster. *Geophysical Research Letters*, *30*(6), 1327. https://doi.org/10.1029/2002GL016500

Shiokawa, K., Nakajima, A., Ieda, A., Sakaguchi, K., Nomura, R., Aslaksen, T., et al. (2010). Rayleigh-Taylor type instability in auroral patches. *Journal of Geophysical Research*, *115*, A02211. https://doi.org/10.1029/2009JA014273

Shiokawa, K., Shiokawa, K., Hashimoto, A., Hori, T., Sakaguchi, K., Ogawa, Y., et al. (2014). Auroral fragmentation into patches. *Journal of Geophysical Research: Space Physics*, *119*, 8249–8261. https://doi.org/10.1002/2014JA020050

Spence, H. E., Kivelson, M. G., Walker, R. J., & McComas, D. J. (1989). Magnetospheric plasma pressures in the midnight meridian: Observations from 2.5 to 35 R_E. *Journal of Geophysical Research*, *94*, 5264–5272.

Takahashi, K., & Ukhorskiy, A. Y. (2007). Solar wind control of Pc5 pulsation power at geosynchronous orbit. *Journal of Geophysical Research*, *112*, A11203. https://doi.org/10.1029/2007JA012483

Treumann, R. A., & Baumjohann, W. (1997). *Advanced space plasma physics*. London: Imperial College Press.

Voronkov, I., Donovan, E. F., Jackel, B. J., & Samson, J. C. (2000). Large-scale vortex dynamics in the evening and midnight auroral zone: Observations and simulations. *Journal of Geophysical Research*, *105*(A8), 18,505–18,518.

Zhu, X., & Kivelson, M. G. (1991). Compressional ULF waves in the outer magnetosphere 1. Statistical study. *Journal of Geophysical Research*, *96*(A11), 19,451–19,467.